A modular numerical method for implicit 0D/3D coupling in cardiovascular finite element simulations

Article *in* Journal of Computational Physics · January 2012

DOI: 10.1016/j.jcp.2012.07.035

4 authors:

Mahdi Esmaily Moghadam
University of California, San Diego
38 PUBLICATIONS **1,214** CITATIONS
SEE PROFILE

Irene E Vignon-Clementel
National Institute for Research in Computer Science and Control
134 PUBLICATIONS **4,407** CITATIONS
SEE PROFILE

Richard Figliola
Clemson University
100 PUBLICATIONS **2,488** CITATIONS
SEE PROFILE

Alison L Marsden
Stanford University
259 PUBLICATIONS **6,216** CITATIONS
SEE PROFILE

Journal of Computational Physics 244 (2013) 63–79

Contents lists available at SciVerse ScienceDirect

Journal of Computational Physics

journal homepage: www.elsevier.com/locate/jcp

A modular numerical method for implicit 0D/3D coupling in cardiovascular finite element simulations

Mahdi Esmaily Moghadam [a], Irene E. Vignon-Clementel [b], Richard Figliola [c], Alison L. Marsden [a,*], for the Modeling Of Congenital Hearts Alliance (MOCHA) Investigators [1]

[a] Mechanical and Aerospace Engineering, USCD, San Diego, CA, USA
[b] INRIA Paris-Rocquencourt, Le Chesnay, France
[c] Mechanical Engineering, Clemson University, Clemson, SC, USA

ARTICLE INFO

Article history:
Received 18 November 2011
Accepted 23 July 2012
Available online 7 August 2012

Keywords:
Lumped parameter network
Neumann
Dirichlet
Boundary condition
Backflow stabilization
Patient-specific blood flow
Navier–Stokes FEM solver
Multi-domain method
Multi-scale modeling

ABSTRACT

Implementation of boundary conditions in cardiovascular simulations poses numerical challenges due to the complex dynamic behavior of the circulatory system. The use of elaborate closed-loop lumped parameter network (LPN) models of the heart and the circulatory system as boundary conditions for computational fluid dynamics (CFD) simulations can provide valuable global dynamic information, particularly for patient specific simulations. In this paper, the necessary formulation for coupling an arbitrary LPN to a finite element Navier–Stokes solver is presented. A circuit analogy closed-loop LPN is solved numerically, and pressure and flow information is iteratively passed between the 0D and 3D domains at interface boundaries, resulting in a time-implicit scheme. For Neumann boundaries, an implicit method, regardless of the LPN, is presented to achieve the desired stability and convergence properties. Numerical procedures for passing flow and pressure information between the 0D and 3D domains are described, and implicit, semi-implicit, and explicit quasi-Newton formulations are compared. The issue of divergence in the presence of backflow is addressed via a stabilized boundary formulation. The requirements for coupling Dirichlet boundary conditions are also discussed and this approach is compared in detail to that of the Neumann coupled boundaries. Having the option to select between Dirichlet and Neumann coupled boundary conditions increases the flexibility of current framework by allowing a wide range of components to be used at the 3D–0D interface.

1. Introduction

Due to the involvement of a vast range of length scales, complex geometry, and circulatory dynamics, accurate modeling and numerical stability remain significant challenges in the study of cardiovascular flow. While small vessels and capillaries contribute the majority of total vascular resistance in each organ, and generally determine the direction of the flow in large vessels, most flow features of clinical interest develop inside large vessels, and thus both domains are required for an

* Corresponding author. Tel.: +858 822 3744.
E-mail addresses: mesmaily@ucsd.edu (M. Esmaily Moghadam), Irene.Vignon-Clementel@inria.fr (I.E. Vignon-Clementel), fgliola@clemson.edu (R. Figliola), amarsden@ucsd.edu (A.L. Marsden).

[1] MOCHA Investigators: Edward Bove MD and Adam Dorfman MD (University of Michigan, USA); Andrew Taylor MD, Alessandro Giardini MD, Sachin Khambadkone MD, Marc de Leval MD, Silvia Schievano PhD, and T-Y Hsia MD (Institute of Child Health, UK); G. Hamilton Baker MD and Anthony Hlavacek (Medical University of South Carolina, USA); Francesco Migliavacca PhD, Giancarlo Pennati PhD, and Gabriele Dubini PhD (Politecnico di Milano, Italy); Richard Figliola PhD and John McGregor PhD (Clemson University, USA); Alison Marsden PhD (University of California, San Diego, USA); Irene Vignon-Clementel PhD (INRIA, France), Jeffrey A. Feinstein (Stanford University, USA).

0021-9991/$ - see front matter © 2012 Elsevier Inc. All rights reserved.
http://dx.doi.org/10.1016/j.jcp.2012.07.035

accurate representation of cardiovascular flow dynamics. In addition, accurate values of absolute pressure in the large vessels, which are also highly dependant on boundary conditions, are important for obtaining clinically relevant results from fluid-structure interaction simulations. Computational fluid dynamics (CFD) simulations have been used extensively to model blood flow in large vessels (e.g. [1–4]). Although these studies provide useful spatial and temporal information in the large vessels, their accuracy largely relies on the accuracy of the downstream circulation model imposed through the boundary conditions. Due to computational cost and lack of image resolution for reconstruction, it is currently impossible to include entire complex vascular networks in 3D patient specific models. Thus, to incorporate all relevant scales into a unified model, a multi-domain approach must be utilized, where the temporal and spatial flow behavior is predicted for large vessels in the 3D domain, and the contribution of the numerous small vessels is predicted by a computationally efficient lower order lumped parameter model.

The heart and vessels that are not included in the 3D domain are often modeled as a 0D lumped parameter circuit network including resistor, capacitor, inductor, and diode elements [5]. The temporal behavior of the 0D model is represented by a set of ODE's, derived from the analogous electrical circuit representation of the LPN components. The coupling between the 3D domain and the reduced order model must ensure conservation of mass, which imposes constraints on flow rates, and continuity of pressure or normal stress. However, it is known that this can lead to the imposition of defective boundary conditions [6] and problems of well-posedness [6,7].

In general, coupling between the 3D domain and a lower order 1D or 0D model can be done using either a monolithic or a partitioned approach. In a monolithic approach, the complete coupled system is solved simultaneously, either by analytic implementation of the lower order model, or by numerical integration. A simple 0D model with a known analytical solution can be directly implemented inside the 3D solver as a 'hard coded' boundary condition, with a monolithic implementation of the Dirichlet–Neumann operator [8]. Monolithic implementation of open-loop coupled boundary conditions, such as resistance, Windkessel (RCR), impedance, or simple heart models, in which the relation between the pressure (normal stress) and the flow rate of this boundary is precisely known, has been demonstrated for up to second order ODEs, including coronary artery models [9–11]. However from a practical point of view, any modification to these hard-coded boundary conditions requires detailed end-user knowledge of the 3D solver and intrusive implementation. A modular, and easily modifiable system for coupling an arbitrary LPN network to a 3D solver is therefore desirable, as it increases applicability to a variety of disease applications, and does not require end-user modification of the 3D solver. Similarly, when the 0D network is more complex, leading to higher order or nonlinear networks of ODEs or coupling of multiple outlets the 'Dirichlet–Neumann' operator must be computed numerically if there is no analytical solution for the ODE system. The monolithic coupling approach has been compared in detail to its explicit-in-time counterpart, in the context of fractional step methods [12]. The monolithic solution of such a 3D–0D coupled system requires a significant change in the 3D solver, and may lead to an ill-conditioned numerical system, unless proper care is taken for its preconditioning [13,14].

An alternative to the fully coupled monolithic schemes is the partitioned approach, which has been the focus of much work in the last decade. In the partitioned approach, having a separate solver for the 0D domain enables us to relate flow rates and pressures at the coupled boundaries for any arbitrary closed-loop, high order, nonlinear LPN, with a wide range of components such as diodes and nonlinear resistors. Such an approach facilitates the use of existing solvers and allows for the use of different numerical schemes in the 0D and 3D domains. With the partitioned approach, coupling in time between the 3D and the reduced (0D or 1D) domains can be either explicit, at one extreme, or implicit at the other. This choice may be motivated by the time-step requirement of the Navier–Stokes solver, which must be sufficiently small to use an explicit method [15], or by issues of numerical stability.

Several recent studies have used a partitioned approach with implicit staggered schemes. In most of these studies a backward Euler scheme is used for the time discretization of the 3D model and an implicit discretization is used for the reduced model. Gauss-Seidel schemes with a number of sub-iterations between the higher dimensional domain and the reduced model domain have been proposed [6]. However, for realistic flow values, this approach has been found to require too many sub-relaxation steps [13]. More recently, some partitioned strategies have used a general heterogeneous coupling approach in which average quantities are passed at the interface [16,17]. A proof of concept was demonstrated on multiple 3D domains representing a bifurcating carotid artery [17]. In the coupling method proposed in [16], two nonlinear iteration loops were required. These studies also advocated use of Newton methods to achieve convergence. In another previous study, a cycle by cycle open-loop simulation was used, and the outlet boundary conditions were corrected to re-balance outlet flow rates [18]. Despite this recent work, the effectiveness of an iterative implicit coupled approach with complex closed-loop LPNs, in which simultaneous temporal data in the LPN is required, has not been established yet. As noted in [15], these systems may suffer from ill-conditioning, and special care must be taken to ensure numerical stability.

In the present work, a time-implicit approach is proposed to couple the Navier–Stokes equations solved in the 3D domain, to complex closed-loop 0D models. This overcomes current limitations related to the numerical instability and restrictive time step choices. The contributions of the coupling to both the tangent matrix and the residual vector are evaluated with an independent code. The Dirichlet–Neumann operator is thus numerically, rather than analytically, determined. With proper communication protocols between the two domains, this approach provides much higher flexibility for modeling the entire circulatory system, with no requirement for modification or intrusion into the 3D solver, once the coupling framework has been implemented. Hence this method incorporates attractive features of both monolithic and partitioned approaches. The adopted time discretization scheme is second order accurate or higher, and allows both domains to be marched in time simultaneously using a predictor-corrector algorithm. This facilitate use of a implicit integration scheme in the 0D domain.

We also aim to overcome previous restrictions that required use of only Neumann boundary conditions in the 3D domain, by expanding our formulation to include Dirichlet coupling. This offers greater flexibility in choosing LPN components, yet maintains the well-posedness of the problem. Based on the selected component at the 3D–0D interface, which is dictated by the physiological relevance of the LPN, a Dirichlet or Neumann boundary condition can be used. In previous approaches, to couple a heart model to the 3D domain, a combination of Dirichlet and Neumann boundary conditions with an augmented Lagrangian constraint was used. While this approach allows one to prescribe a physiologic flow profile during systole, it requires appropriate numerics to perform the switching, and is associated with increased implementation complexity, and higher computational cost [10,19]. Here, the coupling is applied as a Dirichlet condition, with a chosen velocity profile. The coupling term in this case is not strictly a part of the variational formulation, since it is an essential boundary condition that changes at each nonlinear iteration of the 3D solver, according to the 0D numerical solution.

Neumann boundaries are vulnerable to numerical instabilities caused by backflow, which is inevitable and physiologic for many cardiovascular applications such as the ascending aorta. Considering these challenges, we incorporate a new relatively non-intrusive and robust method that relies on a stabilized formulation in the presence of inward flow, therefore expanding the practicality of Neumann boundaries to a wider range of problems [19]. Therefore with the introduced coupling method, based on user preference, a Neumann or Dirichlet boundary condition can be used to couple the lumped heart model to the 3D domain.

The paper is organized as follows: we first introduce the essential multi-domain formulation for coupling any arbitrary 0D domain to a 3D finite element discretized domain. Two possible methods for coupling 0D and 3D domains, i.e. using modified classical Neumann and Dirichlet boundary conditions, and important considerations related to both of these methods are discussed. To the best of our knowledge, this represents the first study of heterogeneous multi-domain coupling, in which these two variations are discussed and compared. Therefore, we make a detailed comparison of the pros and cons of these methods, in which we contrast the effects of increasing LPN contribution to the tangent matrix. The stability, accuracy, and cost of the numerical method presented here are established through multiple case studies.

2. Methods

In this work, we solve a coupled problem in which the Navier–Stokes equations of blood flow in a 3D domain are numerically coupled to a system of ODE's in a 0D domain. Both systems are solved numerically, with appropriate information exchange in each time step at the coupled boundaries. We first describe the numerical methods used for each domain and then describe the coupling algorithm.

2.1. 3D solver formulation

In this work the fluid is considered to be incompressible and Newtonian with a rigid wall assumption. The Navier–Stokes equations are,

$$\rho\dot{\boldsymbol{u}} + \rho\boldsymbol{u}\cdot\nabla\boldsymbol{u} - \nabla\cdot\boldsymbol{T} - \boldsymbol{f} = 0,$$

$$\nabla\cdot\boldsymbol{u} = 0, \tag{1}$$

$$\boldsymbol{T} = -p\boldsymbol{I} + \mu(\nabla\boldsymbol{u} + \nabla\boldsymbol{u}^T), \tag{2}$$

$$\boldsymbol{u} = \boldsymbol{g}, \quad \boldsymbol{x}\in\Gamma_g, \tag{3}$$

$$\boldsymbol{T}\cdot\boldsymbol{n} = \boldsymbol{h}, \quad \boldsymbol{x}\in\Gamma_h, \tag{4}$$

where $\rho, \dot{\boldsymbol{u}} = \dot{\boldsymbol{u}}(\boldsymbol{x},t),\ \boldsymbol{u} = \boldsymbol{u}(\boldsymbol{x},t),\ p = p(\boldsymbol{x},t),\ \boldsymbol{f} = \boldsymbol{f}(\boldsymbol{x},t)$, and $\boldsymbol{T}$ are the density, velocity time derivative taken with respect to a fixed spatial location, velocity vector, pressure, body forces vector, and stress tensor, respectively. In Eqs. (3) and (4), the Neumann and Dirichlet boundaries are denoted by Γ_h and Γ_g, respectively. As shown in Fig. 1, these boundaries can be split to coupled and uncoupled domains, $\Gamma_h = \Gamma_{h_c}\cup\Gamma_{h_u}$ and $\Gamma_g = \Gamma_{g_c}\cup\Gamma_{g_u}$. Note that for the coupled boundaries, $\boldsymbol{g} = \boldsymbol{g}(\boldsymbol{u},p;\boldsymbol{x},t)$ and $\boldsymbol{h} = \boldsymbol{h}(\boldsymbol{u},p;\boldsymbol{x},t)$ are computed based on the 0D domain behavior, whereas for the uncoupled boundaries $\boldsymbol{g} = \boldsymbol{g}(\boldsymbol{x},t)$ and $\boldsymbol{h} = \boldsymbol{h}(\boldsymbol{x},t)$ are prescribed values.

The equivalent weak form of Eqs. (1)–(4) is: find $\boldsymbol{u}\in\left\{\boldsymbol{u}|\boldsymbol{u}(\boldsymbol{x},t)\in(H^1)^d\times[0,T],\ \boldsymbol{u} = \boldsymbol{g}\text{ on }\Gamma_g\right\}$ and $p\in\left\{p|p(\boldsymbol{x},t)\in L^2\times[0,T];\ \text{if }\Gamma=\Gamma_g\text{then}\int_\Omega p\mathrm{d}\Omega = 0\right\}$, such that for all $\boldsymbol{w}\in\left\{\boldsymbol{w}|\boldsymbol{w}(\boldsymbol{x},t)\in(H^1)^d\times[0,T],\ \boldsymbol{w} = 0\text{ on }\Gamma_g\right\}$ and $q\in\left\{q|q(\boldsymbol{x},t)\in L^2\times[0,T]\right\}$,

$$B(\boldsymbol{w},q;\boldsymbol{u},p) = \int_\Omega \boldsymbol{w}\cdot(\rho\dot{\boldsymbol{u}} + \rho\boldsymbol{u}\cdot\nabla\boldsymbol{u} - \boldsymbol{f})\mathrm{d}\Omega + \int_\Omega \nabla\boldsymbol{w}:\boldsymbol{T}\mathrm{d}\Omega + \int_\Omega q\nabla\cdot\boldsymbol{u}\mathrm{d}\Omega - \int_{\Gamma_h}\boldsymbol{w}\cdot\boldsymbol{h}\mathrm{d}\Gamma = 0. \tag{5}$$

In the discrete setting, we make use of a stabilized formulation (see, e.g. [20–23]), which allows equal-order velocity and pressure interpolation, and addresses the convective instability associated with Galerkin's method. The weak form in Eq. (5) is discretized in space with linear finite elements.

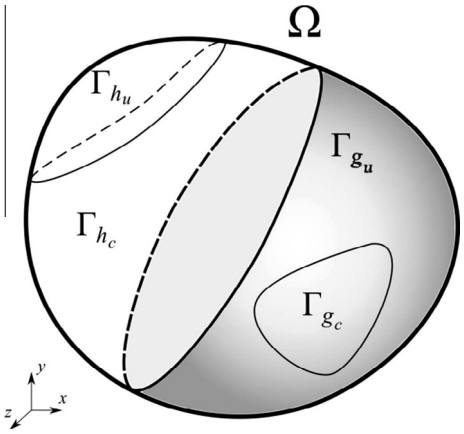

Fig. 1. Schematic of the Neumann, $\Gamma_h = \Gamma_{h_c} \cup \Gamma_{h_u}$, and Dirichlet, $\Gamma_g = \Gamma_{g_c} \cup \Gamma_{g_u}$, boundaries, each divided into coupled and uncoupled boundaries. Ω is the entire 3D computational domain and $\Gamma_h \cup \Gamma_g = \partial\Omega$.

After discretizing these equations, the residual vector can be obtained from Eq. (5) since it should hold for any w_i and q. Using the second order generalized-α method for the time integration of these nonlinear ODE's [24] and a modified Newton–Raphson method for their linearization, the following algebraic system is obtained,

$$\boldsymbol{K}\boldsymbol{Y} = -\boldsymbol{R}, \tag{6}$$

$$\boldsymbol{K} = \begin{bmatrix} \widetilde{\boldsymbol{K}} & \boldsymbol{G} \\ \boldsymbol{D} & \boldsymbol{L} \end{bmatrix} \simeq \begin{bmatrix} \frac{\partial \boldsymbol{R}_m}{\partial \Delta \dot{\boldsymbol{U}}} & \frac{\partial \boldsymbol{R}_m}{\partial \Delta \boldsymbol{P}} \\ \frac{\partial \boldsymbol{R}_c}{\partial \Delta \dot{\boldsymbol{U}}} & \frac{\partial \boldsymbol{R}_c}{\partial \Delta \boldsymbol{P}} \end{bmatrix}, \tag{7}$$

$$\boldsymbol{Y} = \begin{bmatrix} \Delta \dot{\boldsymbol{U}} \\ \Delta \boldsymbol{P} \end{bmatrix}, \tag{8}$$

$$\boldsymbol{R} = \begin{bmatrix} \boldsymbol{R}_m \\ \boldsymbol{R}_c \end{bmatrix}, \tag{9}$$

where $\boldsymbol{R}_m$ and $\boldsymbol{R}_c$ are the momentum and continuity residual vectors, and $\dot{\boldsymbol{U}}$ and $\boldsymbol{P}$ are vectors discretized in space, containing the time derivative of velocity and pressure, respectively, and $\boldsymbol{K}$ is the tangent (stiffness) matrix. This system is solved in each time step and nonlinear Newton iteration with a combination of a conjugate gradient method and a preconditioned Generalized Minimum Residual (GMRES) method. The spectral radius of infinite time step, so called ρ_∞, set to 0.2 for all simulations. For more details about the discretization, linearization and linear solvers, see [24,25].

To create the 3D model geometries a customized in-house version of the open source Simvascular software package is used [26]. The model is meshed with tetrahedral elements using the commercial package MeshSim© Simmetrix, Clifton Park, NY. A custom finite element code is used for the simulations [20]. Experimental validation of the CFD solver in a cardiovascular context is discussed in [27]. Blood density and viscosity are set to be 1060 Kg/m^3 and 0.004 Pa s. The time step size for the 3D solver will be specified for each test case. Nonlinear iterations are performed until the average second norm of the residual vector is less than 5×10^{-4} or the number of iterations exceeds 45.

2.2. Strongly coupled iterative multi-domain formulation

For each LPN, we use a circuit analogy in which current and voltage are analogous to flow and pressure, and resistors, capacitors, diodes, and inductors represent the resistance to flow, distensibility of the vessels, valves, and flow inertia, respectively [5]. Each LPN is described by a set of ODEs.

The multi-domain approach presented here should seamlessly integrate the 3D domain, where spatial and time dependent data are computed, with the 0D domain, where only time dependent data are desired. Since the uncoupled Neumann and Dirichlet boundaries are prescribed in time and space, the velocity and pressure field in the 3D domain can be solved via Eq. (5) once the coupled boundaries $\boldsymbol{h},\ \forall \boldsymbol{x} \in \Gamma_{h_c}$ and $\boldsymbol{g},\ \forall \boldsymbol{x} \in \Gamma_{g_c}$ are known.

Let us define the coupled Neumann and Dirichlet boundary indices as $\eta_h = \{1, 2, \ldots, n_h\}$ and $\eta_g = \{1, 2, \ldots, n_g\}$, where n_h and n_g are the number of coupled Neumann and Dirichlet boundaries, respectively. The flow rate and spatially averaged pressure of the coupled boundaries are defined as,

$$Q_i(t) = \int_{\Gamma_i} \boldsymbol{u}\cdot\boldsymbol{n}\mathrm{d}\Gamma, \tag{10}$$

$$\mathcal{P}_i(t) = \frac{\int_{\Gamma_i} p\mathrm{d}\Gamma}{\int_{\Gamma_i}\mathrm{d}\Gamma}, \tag{11}$$

where $\Gamma_i \subset \Gamma_{h_c}\cup\Gamma_{g_c},\ i\in\eta_h\cup\eta_g$ is the boundary of the surface i. Based on these values, $\boldsymbol{h}$ and $\boldsymbol{g}$ for the coupled surfaces are defined as,

$$\boldsymbol{h}(\boldsymbol{u},p;\boldsymbol{x},t) = -\mathcal{P}_i\boldsymbol{n}, \quad \boldsymbol{x}\in\Gamma_i,\ i\in\eta_h, \tag{12}$$

$$\boldsymbol{g}(\boldsymbol{u},p;\boldsymbol{x},t) = \frac{\phi(\mathbf{x},\mathbf{t})}{\int_{\Gamma_i}\phi\mathrm{d}\Gamma}Q_i\boldsymbol{n}, \quad \boldsymbol{x}\in\Gamma_i,\ i\in\eta_g, \tag{13}$$

where, $\phi(\boldsymbol{x},t)$ is the prescribed velocity profile. For cases in which we have fully developed axial flow at the coupled surface, and the cross section is not necessarily circular, this function can be approximately replaced by the solution of Poisson's equation with constant source term and zero Dirichlet boundary condition at the wall. For a Newtonian, steady and unidirectional flow, Eq. (1) reduces to [28],

$$\nabla^2\boldsymbol{u} = \frac{1}{\mu}\nabla p, \tag{14}$$

where $\boldsymbol{u}$ is non-zero only in the axial direction (i.e. along the vessel centerline) and pressure gradient is constant for that direction. Replacing $\boldsymbol{u}\cdot\boldsymbol{n}$ with ϕ, Eq. (14) is a Poisson equation with constant source term, which must be zero at walls due to the no-slip boundary condition.

Some 0D models, such as resistance and Windkessel [9] models, are simple enough that the relation between the boundary traction and surface flow rate, can be explicitly derived. For these types of boundary conditions $\mathcal{P}_i$ is a function of the flow rate of the same surface only, i.e. $\mathcal{P}_i = \mathcal{P}_i(Q_i),\ i\in\eta_h$. For example, a resistance boundary condition is imposed by $\mathcal{P}_i = RQ_i$.

In general an explicit function does not exist or must be solved numerically for $\mathcal{P}_i,\ i\in\eta_h$ and $Q_i,\ i\in\eta_g$. That relationship can be a nonlinear function of $Q_j,\ j\in\eta_h$ and $\mathcal{P}_k,\ k\in\eta_g$ represented by a system of ordinary differential equations. Hence, a multi-domain approach is used, in which the following system of ordinary differential equations is solved to represent the circulation outside of the 3D domain,

$$\dot{\boldsymbol{\mathcal{X}}} = \widetilde{\boldsymbol{A}}\boldsymbol{\mathcal{X}} + \tilde{\boldsymbol{b}}(Q_i,\mathcal{P}_j,t), \quad i\in\eta_h,\ j\in\eta_g, \tag{15}$$

to find $\mathcal{P}_i,\ i\in\eta_h$ and $Q_i,\ i\in\eta_g$ of the coupled boundaries,

$$\mathcal{P}_i = \mathcal{P}_i(Q_j,\mathcal{P}_k,\mathcal{X}_l,t), \quad i,j\in\eta_h,\ k\in\eta_g,\ l\in\eta_{\mathcal{X}}, \tag{16}$$

$$Q_i = Q_i(Q_j,\mathcal{P}_k,\mathcal{X}_l,t), \quad j\in\eta_h,\ i,k\in\eta_g,\ l\in\eta_{\mathcal{X}}, \tag{17}$$

where, $\mathcal{X}_i$ are the unknowns in the 0D domain and $\eta_{\mathcal{X}}$ is their corresponding index set. Generally unknowns in the 0D domain are selected such that, $\{Q_i,\mathcal{P}_j\}\subset\boldsymbol{\mathcal{X}}$ for $i\in\eta_g,\ j\in\eta_h$.

The data passed between the two domains is shown schematically in Fig. 2. The first type of coupling is when flow rate is passed from the 3D to the 0D domain, and pressure is passed from the 0D to the 3D domain to impose the traction via Eqs. (5) and (12). This type of coupling will be referred to as 'Neumann coupling'. We note that due to the coupling this boundary condition is not strictly a classic Neumann condition. The second type of coupling is when pressure is passed from the 3D to the 0D domain and flow rate is passed back to the 3D domain to impose a spatial velocity profile via Eq. (13). This type of coupling will be referred to as 'Dirichlet coupling'. In some situations, we may have all of one type (either Dirichlet or Neumann) or we may have a mix of two types of boundaries in the same model. In our formulation these data are exchanged between the two domains at each Newton iteration of the nonlinear Navier–Stokes solver to ensure convergence of both domains simultaneously.

In the discrete setting the linearized version of Eq. (15) is solved for time advancement in the 0D domain. This can be represented by,

$$\boldsymbol{A}\boldsymbol{\mathcal{X}}^{\tilde{n}+1} = \boldsymbol{b}(\boldsymbol{\mathcal{X}}^{\tilde{n}},Q_i^m,\mathcal{P}_j^m,t), \quad i\in\eta_h,\ j\in\eta_g,\ m\in\{n,n+1\}, \tag{18}$$

where $\tilde{n}$ and n denote the time steps in the 0D and 3D domains, respectively. This system of ODEs representing the LPN is advanced in time with a 4th order Runge–Kutta method in this study. Since the integration of Eq. (18) is cheap relative to the 3D domain time-advancement, the time between n and $n+1$ is split into 1000 0D-domain sub-time steps to increase accuracy and prevent potential sources of instability emanating from the 0D domain.

At the start of the simulation, the 0D and 3D domains are initialized with $\boldsymbol{\mathcal{X}}^1$ and $\{\boldsymbol{U}^1,\boldsymbol{P}^1\}$, respectively. In the generalized-α method, the solution at n is fixed and the solution at $n+1$ is corrected after each nonlinear Newton–Raphson iteration [24]. In each time step, from n to $n+1$ in the 3D domain, the following steps are performed:

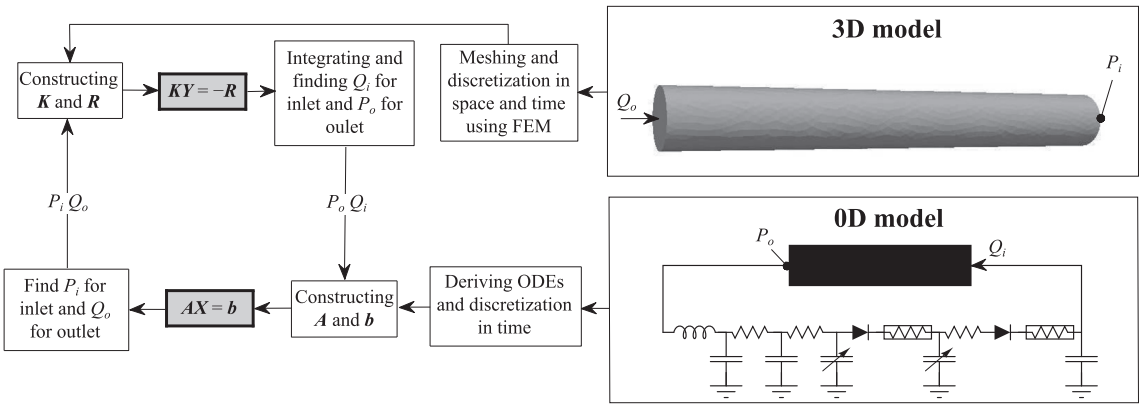

Fig. 2. Schematic of strongly coupled iterative multi-domain solver. In the 0D domain ODEs, discretized in time, can be solved by receiving the flow rate of coupled Neumann surfaces and pressure of coupled Dirichlet surfaces from the 3D domain. The 3D domain, discretized in space and time, requires the pressure of coupled Neumann surfaces and flow rate of coupled Dirichlet surfaces from the 0D domain to solve the linearized N-S equations. In this schematic, $\boldsymbol{A}\mathcal{X} = \boldsymbol{b}$, and $\boldsymbol{KY} = -\boldsymbol{R}$ are the linearized system of equations solved in the 0D and 3D domains, respectively.

1. Predict unknowns at time step $n+1$ and iteration kth in the 3D domain based on the solution at time step n,

$$k = 0, \tag{19}$$

$$\boldsymbol{U}_{(k)}^{n+1} = \boldsymbol{U}^{n}, \tag{20}$$

$$\boldsymbol{P}_{(k)}^{n+1} = \boldsymbol{P}^{n}. \tag{21}$$

2. Use Eqs. (10) and (11) to compute the flow rate, $\{Q_i^n, Q_{i(k)}^{n+1}\}\ \forall i \in \eta_h$, and pressure of coupled boundaries, $\{\mathcal{P}_i^n, \mathcal{P}_{i(k)}^{n+1}\}\ \forall i \in \eta_g$, and pass them to the 0D domain.
3. After receiving the flow and pressure data at time steps n and $n+1$ in the 0D domain and retrieving $\boldsymbol{\mathcal{X}}^n$ as the starting point of integration, integrate the ODE's up to $n+1$, using Eq. (18).
4. After receiving $\mathcal{P}_{i(k)}^{n+1}\ \forall i \in \eta_h$ and $Q_{i(k)}^{n+1}\ \forall i \in \eta_g$ from the 0D domain, calculate the traction at the coupled Neumann boundaries and the nodal velocities at the coupled Dirichlet boundaries by using Eqs. (12) and (13), respectively.
5. Use Eqs. (5)–(9) to construct $\boldsymbol{R}$ and $\boldsymbol{K}$ and solve the linearized Navier–Stokes equations to find $\Delta\dot{\boldsymbol{U}}$ and $\Delta\boldsymbol{P}$.
6. Correct velocity and pressure in the 3D domain, using,

$$\boldsymbol{P}_{(k+1)}^{n+1} = \boldsymbol{P}_{(k)}^{n+1} + \alpha_f \gamma \Delta t \Delta\tilde{\boldsymbol{P}}, \tag{22}$$

$$\boldsymbol{U}_{(k+1)}^{n+1} = \boldsymbol{U}_{(k)}^{n+1} + \gamma \Delta t \Delta\dot{\boldsymbol{U}}, \tag{23}$$

$$\dot{\boldsymbol{U}}_{(k+1)}^{n+1} = \dot{\boldsymbol{U}}_{(k)}^{n+1} + \Delta\dot{\boldsymbol{U}}. \tag{24}$$

The time integration coefficients used in these equations can be different, depending on the formulation used in constructing $\boldsymbol{K}$. $\Delta\tilde{\boldsymbol{P}} = \frac{\Delta\boldsymbol{P}}{\alpha_f \gamma \Delta t}$ in Eq. (22) is a change of variable to obtain anti-symmetric blocks in Eq. (7), i.e. $\boldsymbol{D} = -\boldsymbol{G}^t$. α_f and γ are the generalized-α method coefficients, calculated based on ρ_∞.

7. Set $k \leftarrow k+1$ and go back to the second step if the residual is not small enough, $\|\boldsymbol{R}\|_2 > \epsilon$, or the number of iterations has not exceeded the maximum specified value, $k > k_{max}$.
8. Before going to the next 3D-domain time step, calculate $\boldsymbol{\mathcal{X}}^{n+1}$ based on the corrected flow rate and pressure. Then set $n \leftarrow n+1$ and go back to the first step.

Compared to the method implemented in [15], the coupling in our approach is implicit in time (Fig. 3). This framework therefore offers the flexibility to use either an implicit or explicit time-integration method in the 0D domain.

2.2.1. Remarks on coupling the Neumann boundaries

In the case of a coupled Neumann boundary, the pressure is passed from the 0D to the 3D domain, and flow rates are passed from the 3D to the 0D domain. If the circuit element directly connected to the coupled boundary is a capacitor, then using the presented numerical scheme it is essential to assign a Neumann boundary to avoid instabilities (see appendix). In this case, the flow rate is a natural forcing term in the ODE system of equations, whereas pressure is a state variable. This type of boundary condition, as opposed to the Dirichlet boundary condition, does not require a prespecified spatial velocity profile. For the coupled Neumann boundaries, the pressures can be assembled into the discretized residual vector using,

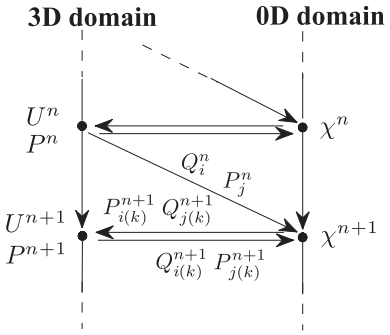

Fig. 3. Schematic of time marching in both 3D and 0D domains. The 0D domain sends corrected $\mathcal{P}_{i(k)}^{n+1}$ and $Q_{j(k)}^{n+1}$ to the 3D domain and receives Q_i^n and $\mathcal{P}_j^n$ and the corrected $Q_{i(k)}^{n+1}$ and $\mathcal{P}_{j(k)}^{n+1}$ values from the 3D domain. In this figure $i \in \eta_h$ and $j \in \eta_g$.

$$(R_m)_{Ai} \leftarrow (R_m)_{Ai} + \int_{\Gamma_j} N_A \mathcal{P}_j^{n+1} n_i \mathrm{d}\Gamma, \quad j \in \eta_h, \tag{25}$$

where $N_A(\boldsymbol{x})$ is the shape function for node A and $i \in \{1, \cdots, \text{number of spatial dimensions}\}$. For the coupled Neumann boundaries, the same Newton approach is used to solve the nonlinear formulation as without the coupling. Hence, the algorithm contains only one nonlinear iteration loop involving the 3D solver. Since the added term to the momentum residual vector in Eq. (25) depends on the velocity, the contribution of the 0D domain can be added to the tangent matrix to obtain a robust implicit scheme. For an implicit coupling, the contribution of the coupled surface terms in the tangent matrix in Eq. (7) is,

$$\widetilde{K}_{AiBj} \leftarrow \widetilde{K}_{AiBj} + \frac{\partial (R_m)_{Ai}}{\partial \Delta \dot{U}_{Bj}}. \tag{26}$$

Using Eqs. (10) and (26), and the fact that $\mathcal{P}_i^{n+1}$ is constant over Γ_i,

$$\widetilde{K}_{AiBj} \leftarrow \widetilde{K}_{AiBj} + \frac{\partial (R_m)_{Ai}}{\partial Q_l^{n+1}} \frac{\partial Q_l^{n+1}}{\partial U_{Ck}^{n+1}} \frac{\partial U_{Ck}^{n+1}}{\partial \dot{U}_{Bj}^{n+1}} = \widetilde{K}_{AiBj} + \gamma \Delta t M_{kl} \int_{\Gamma_k} N_A n_i \mathrm{d}\Gamma \int_{\Gamma_l} N_B n_j \mathrm{d}\Gamma, \tag{27}$$

where the M_{ij} is the $n_h \times n_h$ matrix,

$$M_{ij} = \frac{\partial \mathcal{P}_i^{n+1}}{\partial Q_j^{n+1}}, \quad i,j \in \eta_h. \tag{28}$$

Generally, this matrix is not available analytically. Therefore, it must be calculated numerically row-by-row, in this case using a finite difference method. This is done by passing $Q_j^{n+1} + \epsilon,\ j \in \eta_h$ to the 0D domain, solving for the resulting pressure, and then dividing the change in $\mathcal{P}_i^{n+1},\ i \in \eta_h$ by ϵ. This Jacobian-like matrix is,

$$M_{ij} = \frac{\mathcal{P}_i^{n+1}\left(Q_j^{n+1} + \epsilon; Q_j^n\right) - \mathcal{P}_i^{n+1}\left(Q_j^{n+1}; Q_j^n\right)}{\epsilon}. \tag{29}$$

In above expression, ϵ can be selected as,

$$\epsilon = \max\left\{\epsilon_{abs}, \epsilon_{rel}|Q_j^{n+1}|\right\}, \tag{30}$$

where ϵ_{abs} depends on the machine precision and ϵ_{rel} is chosen based on the accuracy requirements.

Usually the off diagonal entries of M_{ij}, which can be physically interpreted as the effect of changing the flow rate at face j on the pressure at face i, are generally negligible compared to the diagonal terms. Neglecting the off diagonal entries improves the sparsity of the tangent matrix, which can be exploited in the linear solver. This is the choice that was implemented in this work. This matrix is computed only once for a linear LPN. We will compare three cases with increasing levels of contribution to the tangent matrix within each Newton iteration. We refer to the case of update of the matrix at each iteration as the 'implicit' method. We refer to the case of partial update, i.e. when the matrix is computed just once at the start of the simulation, as the 'semi-implicit' method. We refer to the case of no update, i.e. when no contribution is added to the tangent matrix, as the 'explicit' method.

The method described here for the coupled Neumann boundaries can result in numerical instability due to backflow at the coupled faces of the model. This is a well-known problem in cardiovascular simulation, but one that is often overlooked. This problem results when flow is entering the domain without explicit prescription of a velocity profile. In many situations, accurately capturing backflow is essential to reproducing the correct physiological behavior. For example the heart model coupled with the ascending aorta as a Neumann boundary will result in flow entering the domain during the systole without

a prescribed velocity profile. Except for very simple geometries, if the Neumann boundaries are not treated with care, the solution will diverge rapidly. This issue has been addressed in previous works by enforcing a velocity profile using Lagrange constraints, by enforcing normal velocity at the outflow face, or by extending outlets unrealistically using long cylindrical sections [29,30]. Our recent work identified a stable, accurate and non-intrusive method for solving this issue by adding an advective stabilization term to the weak form [19,31]. Therefore, Eq. (5) is modified as,

$$\tilde{B}(\boldsymbol{w},q;\boldsymbol{u},p) = B(\boldsymbol{w},q;\boldsymbol{u},p) - \beta\int_{\Gamma_h}\rho\boldsymbol{w}\cdot\boldsymbol{u}(\boldsymbol{u}\cdot\boldsymbol{n})_-\mathrm{d}\Gamma, \tag{31}$$

where β is a positive coefficient between 0.0 and 1.0, preferably less than 0.5. For small values of β, this method is less intrusive and also stable over a larger range of time steps. In Eq. (31), $(\boldsymbol{u}\cdot\boldsymbol{n})_-$ is defined as,

$$(\boldsymbol{u}\cdot\boldsymbol{n})_- \equiv \frac{\boldsymbol{u}\cdot\boldsymbol{n}-|\boldsymbol{u}\cdot\boldsymbol{n}|}{2} = \begin{cases}\boldsymbol{u}\cdot\boldsymbol{n} & \boldsymbol{u}\cdot\boldsymbol{n}<0,\\ 0 & \boldsymbol{u}\cdot\boldsymbol{n}\geqslant 0.\end{cases} \tag{32}$$

The added term in Eq. (31) is an outward traction, opposite the direction of backflow, which pushes the flow in the direction of the outward normal. Because $(\boldsymbol{u}\cdot\boldsymbol{n})_-$ in Eq. (32) is defined to be zero in outward flow, this term is only active in the presence of flow reversal.

2.2.2. Remarks on coupling the Dirichlet boundaries

The Dirichlet type of boundary condition requires prescription of spatial velocity profile information, which is scaled by the flow rate (received from the 0D domain) via Eq. (13). The pressure and velocity solution inside the 3D domain depends on the chosen velocity profile, $\phi(\boldsymbol{x},t)$, which is typically either a Poiseuille or Womersley profile. Sensitivity of the solution to the chosen profile, however, is problem-specific and varies depending on the interaction between boundary conditions and geometry in the 3D domain.

If the circuit element in the LPN adjacent to the coupled boundary is an inductor, it is essential to assign a Dirichlet boundary condition to obtain a stable solution, as outlined in the appendix. In this case, pressure is a natural forcing term in the ODE system of equations that represents the 0D domain, whereas flow is a state variable. The Dirichlet boundary condition is updated at the beginning of each nonlinear iteration, using the same procedure as for the Neumann boundaries. In this case, no contribution to the tangent matrix is necessary and coupling is time-implicit. The nodal velocities at $n+1$ are computed using Eq. (13) after receiving flow rates at the coupled Dirichlet surface from the 0D domain. Nodal acceleration is then corrected according to the time discretization used here,

$$\dot{U}_{Ai}^{n+1} = \frac{\gamma-1}{\gamma}\dot{U}_{Ai}^{n} + \frac{1}{\gamma\Delta t}(U_{Ai}^{n+1}-U_{Ai}^{n}), \quad A\in\Gamma_{g_c}. \tag{33}$$

If all the coupled boundaries are Dirichlet and there are no Neumann boundaries, an additional constraint is needed in the 3D domain formulation to prevent pressure drift, namely

$$\int_\Omega p\mathrm{d}\Omega = 0, \quad \text{if } \Gamma=\Gamma_g. \tag{34}$$

In this case, the boundary pressures that are sent to the 0D domain are only pressure differences. All relative pressures received in the 0D domain must be added to the mean pressure in the 3D domain, $\overline{\mathcal{P}}$, to get the correct absolute coupling pressure. For this additional mean pressure unknown, the following additional equation is needed in the 0D domain,

$$\sum_{i=1}^{n_g} Q_i = 0. \tag{35}$$

The governing equation for an inductor adjacent to the coupled boundaries in the 0D domain is,

$$L_i\frac{\mathrm{d}Q_i}{\mathrm{d}t} = L_i f_i = \overline{\mathcal{P}} + \mathcal{P}_i - \mathcal{P}_{d_i}, \quad i\in\eta_g, \tag{36}$$

where, as shown in Fig. 4, L_i, f_i, and $\mathcal{P}_{d_i}$ are the inductance, time derivative of coupled surface flow rate, and distal pressure, respectively. Dividing Eq. (36) by L_i and using Eq. (35), one can show that,

$$\overline{\mathcal{P}} = \left(\sum_{i=1}^{n_g}\frac{1}{L_i}\right)^{-1}\sum_{j=1}^{n_g}\frac{\mathcal{P}_{d_j}-\mathcal{P}_j}{L_j}. \tag{37}$$

Denoting $\tilde{f}_i$ as the time derivative of coupled surfaces flow rate computed in the 0D domain based on a coupling pressure when $\overline{\mathcal{P}}=0$,

$$L_i\tilde{f}_i = \mathcal{P}_i - \mathcal{P}_{d_i}, \quad i\in\eta_g \tag{38}$$

and using Eq. (36) one can show that,

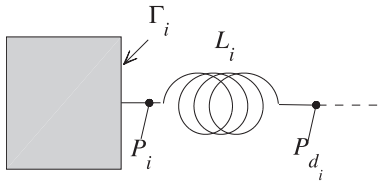

Fig. 4. Schematic of a coupled Dirichlet boundary, Γ_i, coupled via an inductor to the 0D domain. Coupled surface pressure and distal pressure are denoted by $\mathcal{P}_i$ and $\mathcal{P}_{d_i}$, respectively.

$$f_i = \tilde{f}_i - \left(L_i \sum_{j=1}^{n_g} \frac{1}{L_j}\right)^{-1} \sum_{k=1}^{n_g} \tilde{f}_k, \quad i \in \eta_g. \tag{39}$$

Since $\tilde{f}_i$ is found from Eq. (38) with no knowledge of $\overline{\mathcal{P}}$, using Eq. (39), the correct f_i to be imposed in the 3D domain can be calculated.

3. Results

We demonstrate the coupled formulation using three representative cardiovascular problems. The first is a verification exercise in a simple cylinder, the second is a simple closed-loop model with one inlet and one outlet, and the third is a model of a surgery for single ventricle heart patients with a closed-loop complex network and multiple outlets. Both Dirichlet and Neumann methods are demonstrated and compared.

3.1. Verification using a Windkessel model

A cylinder with an unsteady prescribed Dirichlet boundary condition at the inlet, and a Windkessel (RCR) model at the outlet, is considered for verification purposes. The model is shown in Fig. 5, and is meshed with 331,636 tetrahedral elements. In this model R_p, C, R_d, and $Q(t)$ are the proximal resistance, capacitance, distal resistance, and time dependent inflow, respectively.

Prescribing inlet flow rate as $Q = Q_0\left(\sin\left(\frac{t^*}{2}\right)\right)^2$, the pressure at the outlet can be determined analytically as,

$$\frac{P_{ex}}{R_d Q_0} = \left(\frac{R_p}{R_d} + \frac{1}{2}\right)\sin\left(\frac{t^*}{2}\right)^2 + \frac{1}{4}\left(1 - e^{-t^*} - \sin(t^*)\right), \tag{40}$$

where $t^* = \frac{t}{R_d C}$ is the non-dimensional time.

In this simple case, a numerical solution of the 0D model is not necessary since the circuit equation can be solved analytically. For verification purposes, we compare three quantities: (1) the analytical ODE solution (Eq. (40)), (2) the hard-coded RCR coupling (pure monolithic approach [9]), and (3) the numerically coupled solution, using the methods described in this work. There is only one ODE that is time-integrated in the 0D domain to obtain the pressure of the capacitor. In Fig. 6, the analytical solution from Eq. (40) is compared to the coupled 3D–0D simulation results. This simulation is carried out for 1 s with $Q_0 = 10,\ R_p = 0.1,\ R_d = 1.0,\ C = \frac{1}{4\pi}$ in cgs units. The 3D domain time step size is 1 ms and since 1000 time steps per each 3D domain time step is performed, and each Runge–Kutta time step is 1 μs.

Comparing the analytical and numerical results in Fig. 6, the error is less than 1% at all times. The norm of the error, i.e. $100\left\|\frac{P-P_{ex}}{R_d Q_0}\right\|$, for the hard coded and numerical results is 0.42% and 0.46%, respectively. The total simulation time, keeping everything else fixed, was 48 min and 44 min for the monolithic (i.e. hard-coded) and partitioned (i.e. numerically coupled) simulations, respectively.

Considering the small time step size used in the 0D domain, the error due to the 0D integration is negligible. Hence, the small error in Fig. 6 is due to the difference between flow rate at the inlet and outlet of the 3D model. From this figure, the error is proportional to the time derivative of the flow rate. The norm of the mass conservation error, i.e. the difference between the inlet and outlet flow rates is $100\left\|\frac{Q_i - Q_o}{Q_0}\right\|$, equal to 0.024%.

Fig. 5. Windkessel model coupled to a cylinder with an uncoupled Dirichlet inlet boundary condition. The cylinder diameter and length are 4.0 and 30.0 cm, respectively.

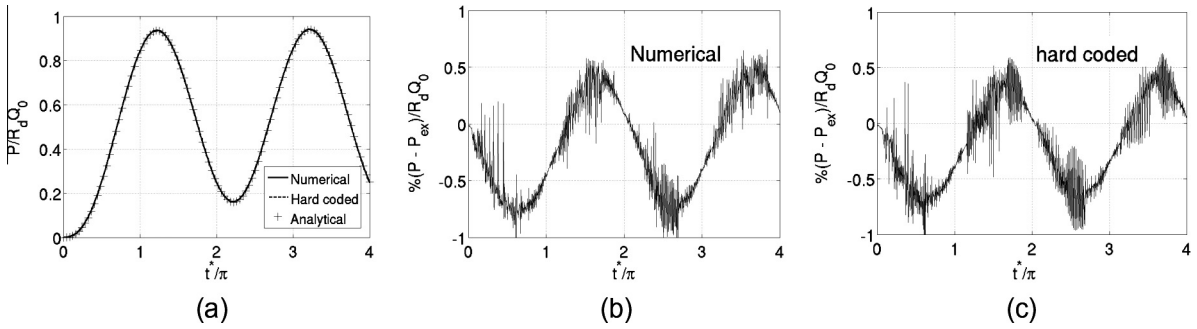

Fig. 6. Cylinder with periodic inflow boundary condition coupled to the Windkessel model shown in Fig. 5, (a) Analytical (+), numerical coupled (solid line) and monolithic or hard coded (dash line) outlet pressures, (b) Normalized error of numerical solution in percent, (c) Normalized error of hard coded solution in percent.

3.2. Closed-loop cylinder model

In this second example both the inlet and outlet of the cylinder are coupled Neumann boundaries. The heart model along with the other blocks of the LPN is shown in Fig. 7. Flow is initiated in the 3D model by the pressure difference produced by the heart model in the LPN. As described in [32] the following relation is assumed between atrial volume, V_a, electrical activation, $A_a(t)$, and atrial pressure, P_a,

$$P_a = A_a E_a (V_a - V_{a_u}) + P_{a_0}\left(e^{K_a(V_a - V_{a_u})} - 1\right). \tag{41}$$

$A_a(t)$ is modeled with a sinusoidal function which is non-zero during atrial contraction and E_a, P_{a_0}, K_a, and V_{a_u} are constants of this model. The same model is used for the ventricle, except the first term in Eq. (41) that models systole, is replaced with a parabolic function,

$$P_v = A_v\left[E_{v_1}(V_v - V_{v_u}) + E_{v_2}(V_v - V_{v_u})^2\right] + P_{v_0}\left(e^{K_v(V_v - V_{v_u})} - 1\right). \tag{42}$$

Eqs. (41) and (42) relate the pressures and volumes of heart chambers. Nonlinear resistances are incorporated into the heart model to account for the pressure drop caused by turbulence in the aortic and tricuspid valves. The parameter values of the heart model and the rest of LPN are shown in Table 1.

The 0D/3D coupled system was solved using 331,636 elements in the 3D domain, for 2.4 s (3 cardiac cycles), with a time step size of 2.4 ms. The pressures at certain points in the LPN, including the coupled surfaces, are shown in Fig. 7. The

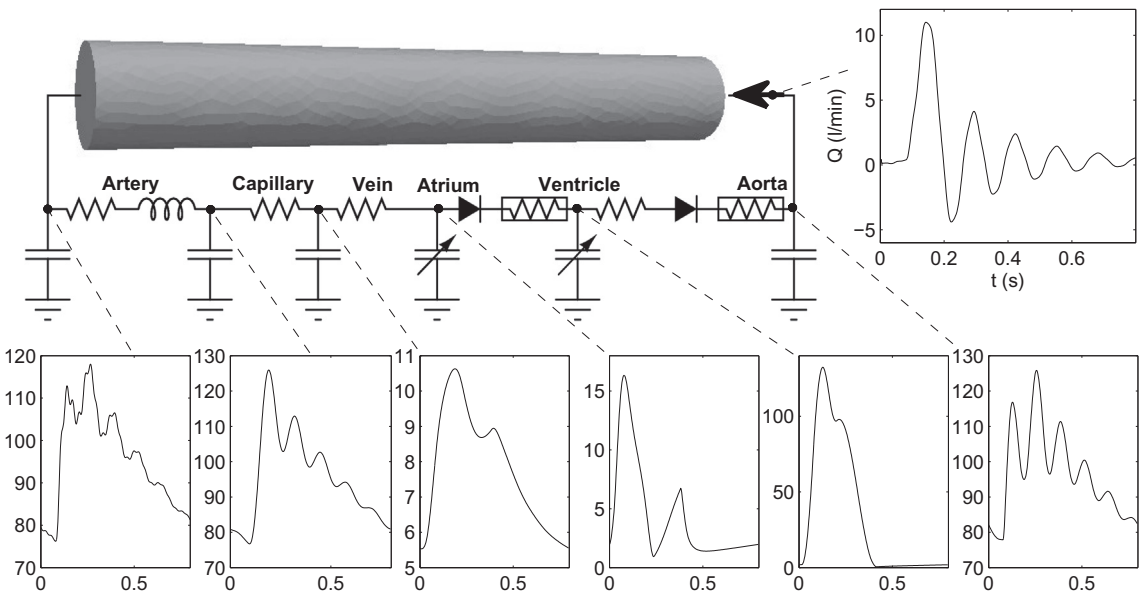

Fig. 7. Lumped parameter network for the coupled cylinder case. This hypothetical model includes six blocks for the systemic artery, capillaries, veins, atrium, ventricle, and aorta. The pressure of certain points in mmHg versus time is plotted. The flow rate at the inlet of the cylinder is also plotted.

Table 1
Fig. 7 parameters values. $\widehat{R}$ are non-linear resistances modeling the heart valves.

Block	Parameter	Value	Unit
Artery	R	0.05	mmHg s/ml
	C	0.02	ml/mmHg
	L	0.004	mmHg s^2/ml
Capillary	R	5.00	mmHg s/ml
	C	0.20	ml/mmHg
Vein	R	0.09	mmHg s/ml
	C	1.00	ml/mmHg
Atrium	$\widehat{R}$	4×10^{-4}	mmHg s^2/ml^2
	E_a	7.35	mmHg/ml
	V_{a_u}	1.0	ml
	P_{a_0}	0.17	mmHg
	K_a	0.484	1/ml
Ventricle	R	0.09	mmHg s/ml
	E_{v_1}	18.5	mmHg/ml
	E_{v_2}	−0.042	mmHg/ml^2
	V_{v_u}	4.0	ml
	P_{v_0}	0.9	mmHg
	K_v	0.062	1/ml
Aorta	$\widehat{R}$	4×10^{-5}	mmHg s^2/ml^2
	C	0.1	ml/mmHg

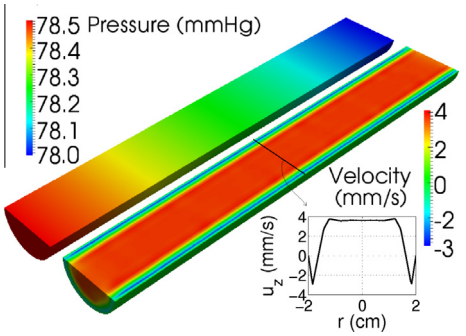

Fig. 8. Contours of pressure and velocity along the cylinder axis of the LPN shown in Fig. 7 during flow acceleration ($t = 1.1T$). The velocity profile for the coupled Neumann boundaries is not imposed, but is a part of the solution. We confirm that the velocity has developed into a Womersley profile with forward flow at the center and backward flow at regions close to the cylinder wall, typical of high Womersley numbers (here 28.8).

interaction between the aortic capacitor in the 0D domain with the fluid inertia in the 3D domain causes aortic pressure oscillations. As expected, this pressure oscillation is damped following the resistive element representing the capillaries. In Fig. 8 a snapshot of pressure and velocity contours is shown for this simulation at $t = 1.1T$.

The results in Fig. 7 correspond to the last cycle of a three cycle simulation. The pressure-volume loop of the heart chambers for all the three cycles is shown in Fig. 9. As shown in this figure, the difference between the second and third cycles is less than the first and second cycles. In this case, due to the accurate initialization of the unknowns in the 0D domain, a few cycles are sufficient to obtain a periodic solution.

3.3. Comparison of the Neumann and Dirichlet coupled boundary approaches

To compare the use of Neumann and Dirichlet coupling methods in terms of stability, accuracy, mesh sensitivity, and computational cost, we consider the coupled model shown in Fig. 7. For the coupled Neumann boundary conditions, we use the model as shown. For the Dirichlet case, to obtain a stable algorithm, we modify the model to include inductors at both the inlet and outlet of the cylinder. For this case, Eq. (39) is used to account for the average pressure from the 3D domain in the 0D domain.

As shown in Tables 2 and 3, the effect of time step size and mesh size are studied and compared for the coupled Neumann and Dirichlet models. For the Neumann cases, the stability of simulations without backflow treatment (i.e. $\beta = 0$) and the effect of including $\boldsymbol{M}$ (Eq. (28)) in the formulation (i.e. I/SI/E) is studied further. Here, the explicit method (E) neglects the contribution of $\boldsymbol{M}$ in the LHS matrix, the semi-implicit method (SI) evaluates $\boldsymbol{M}$ only once at the beginning of the simulation, and the implicit method (I) updates $\boldsymbol{M}$ at each iteration in each time step. A simulation with 331,636 elements, a time step of 0.1 ms, and $\beta = 0.2$ of each corresponding case serves as the reference case in these tables. The results are not reported for the unstable cases.

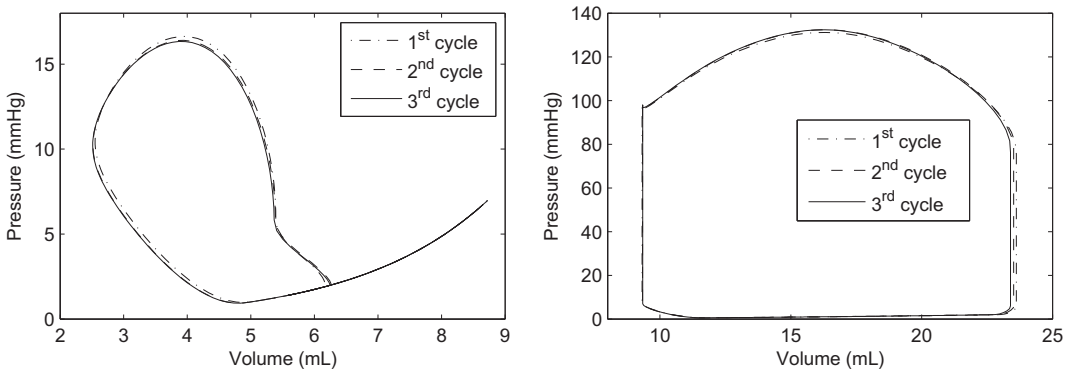

Fig. 9. Atrium (a) and ventricle (b) pressure-volume loops for the LPN shown in Fig. 7. Convergence of the heart model with number of simulated cardiac cycles is shown in this figure.

Table 2
The effect of time step size, left hand side contribution (***M*** in Eq. (28)), stabilization coefficient, and mesh size on the stability and accuracy of the coupled Neumann boundary case. Results of the diverged cases are shown by a dash. Δt: 3D solver time step size in millisecond, I/SI/E: Implicit/Semi-Implicit/Explicit, nEl: Number of elements, β: backflow stabilization coefficient, nIt: Average number of nonlinear iteration needed to reduce second norm of residual to less than 10^{-3}, t_{∞}: Total simulation time in a parallel 8× 2.8 GHz processors machine in minutes. $err = 100\frac{\|Q-Q_{ref}\|_2}{\|Q_{ref}\|_2}$: Normalized aortic flow rate error, as compared to the reference case in percent.

Case	Δt	I/SI/E	β	nEl	nIt	t_{sim}	*err*
N1	1.6	I	0.2	24450	9.1	19.5	7.81
N2	1.6	SI	0.2	24450	9.1	16.3	7.81
N3	1.6	E	0.2	24450	10.2	18.2	7.81
N4	6.4	I	0.2	24450	30.6	16.1	9.83
N5	6.4	SI	0.2	24450	30.1	13.4	9.83
N6	6.4	E	0.2	24450	–	–	–
N7	0.4	SI	0.2	24450	6.3	45.6	8.20
N8	0.4	SI	0.2	109547	5.0	158.4	2.26
N9	0.4	SI	0.2	331636	4.6	438.5	1.10
N10	6.4	SI	0.0	24450	31.3	14.1	20.2
N11	0.4	SI	0.0	24450	–	–	–
N12	0.4	SI	0.0	331636	–	–	–

Table 3
The effect of time step size and mesh size on the stability and accuracy of the coupled Dirichlet boundary case. See Table 2 for abbreviations.

Case	Δt	nEl	nIt	t_{sim}	*err*
D1	32	24450	8.0	0.73	12.6
D2	6.4	24450	6.2	2.68	3.80
D3	1.6	24450	6.0	10.5	3.27
D4	0.4	24450	6.0	42.7	3.47
D5	0.4	109547	4.6	146	0.61
D6	0.4	331636	4.0	389	0.16

The results of these two tables suggest:

1. The accuracy of the coupled Neumann case is independent of the contribution of ***M*** to the tangent matrix as expected.
2. The stability and convergence rate of the coupled Neumann case is improved by switching from the explicit to the semi-implicit. But there is no further improvement gained from switching to an implicit method. This indicates that the time-accumulated contribution of the nonlinear 0D components in a cardiac cycle is negligible compared to the linear components.
3. Using a semi-implicit method can reduce computational cost by improving convergence. However due to the excessive cost of evaluating ***M*** at each iteration, the implicit method is not cost effective.
4. In contrast to the coupled Dirichlet case, the time step size should be limited for the coupled Neumann case to avoid instabilities due to backflow.
5. The stabilized boundary formulation is essential for stability of the Neumann boundaries, especially for smaller time step or mesh sizes.

6. Fewer elements are required to obtain a mesh independent solution for the coupled Dirichlet case as compared to the coupled Neumann case.
7. The coupled Dirichlet case has better convergence rates at larger time step sizes, which is consistent with its lower computational cost.

Combining these observations, we conclude that the Dirichlet boundary condition is the least costly approach, but has the drawback of requiring additional information or assumptions about the velocity profile at the coupled surfaces.

3.4. Single ventricle multi-domain model

In the third example, the first stage surgical anatomy of a hypoplastic left heart syndrome (HLHS) patient is modeled using a multi-domain approach. This surgery, called a Norwood or Blalock Taussig-shunt, is performed to increase oxygenation by shunting a portion of cardiac output to the pulmonary arteries. The LPN along with the anatomy is shown in Fig. 10. In this LPN, there is only one functional ventricle and it is used to pump blood to the aorta. A shunt is inserted between the brachiocephalic artery and the pulmonary artery to supply blood to the lungs. The diameter of the shunt, which should be chosen properly to maintain the ratio of systemic to the pulmonary blood flow at an optimal value, is 3.5 mm in this case study. The AoA, RPA, RCCA, and RCA diameters are 10, 5, 3, and 2.5 mm, respectively. To account for the effect of intramyocardial pressure on the coronary perfusion, the distal end of the capacitor between 'CB' and 'CA2' is connected to the ventricular pressure. Within the current framework, other LPNs can also be used to model coronary circulation [33].

The 3D model is meshed with tetrahedral elements. For the interior, four mesh sizes of 1.0, 0.8, 0.625, and 0.5 mm are selected, that produce approximately 130K, 210K, 400K, and 700K tetrahedral elements, respectively. The mesh size for the coronary artery wall is 40% of the interior mesh size and the mesh size for the rest of the walls is 80% of the interior mesh size. After simulating five cardiac cycles, the differences between the cardiac output with the first three meshes and the last mesh (most refined one) are 2.91%, 0.793%, and 0.524%, respectively. Based on these results, an interior mesh size of 0.625 mm is chosen for this study, which produced a mesh with approximately 400K elements. This example follows previous work of Migliavacca et al., and the parameters in the 0D domain are tuned based on physiological data obtained from a typical set of patients [32].

Since all coupled boundaries are adjacent to capacitors, we use coupled Neumann boundary conditions with a semi-implicit approach for all coupled surfaces. This model is meshed with 400,936 elements. The time step size for the 3D domain is set to 0.5 ms. Since all coupled boundaries of the BT-shunt model exhibit significant backflow during part of the cardiac cycle, these simulations require backflow stabilization, and we set $\beta = 0.2$.

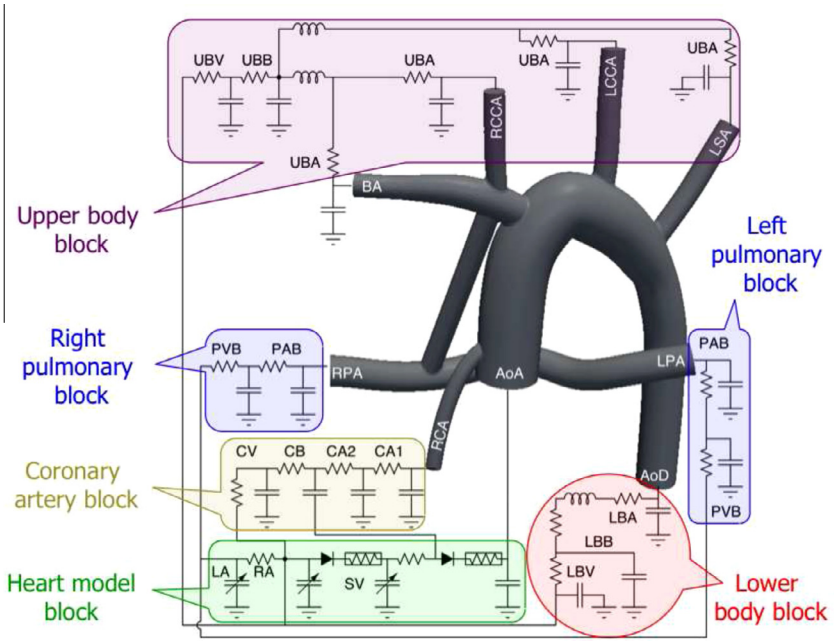

Fig. 10. Postoperative modeling of first stage surgery HLHS patient. AoA: Ascending Aorta, AoD: Descending Aorta, BA: Brachiocephalic Artery, CA: Coronary Artery, CB: Coronary Bed, CV: Coronary Vein, LA: Left Atrium, LBA: Lower Body Artery, LBV: Lower Body Vein, LCCA: Left Common Carotid Artery, LPA: Left Pulmonary Artery, LSA: Left Subclavian Artery, PAB: Pulmonary Artery Bed, PAV: Pulmonary Artery Vein, RA: Right Atrium, RCA: Right Coronary Artery, RCCA: Right Common Carotid Artery, RPA: Right Pulmonary Artery, SV: Single Ventricle. UBA: Upper Body Artery, UBB: Upper Body Bed, UBV: Upper Body Vein.

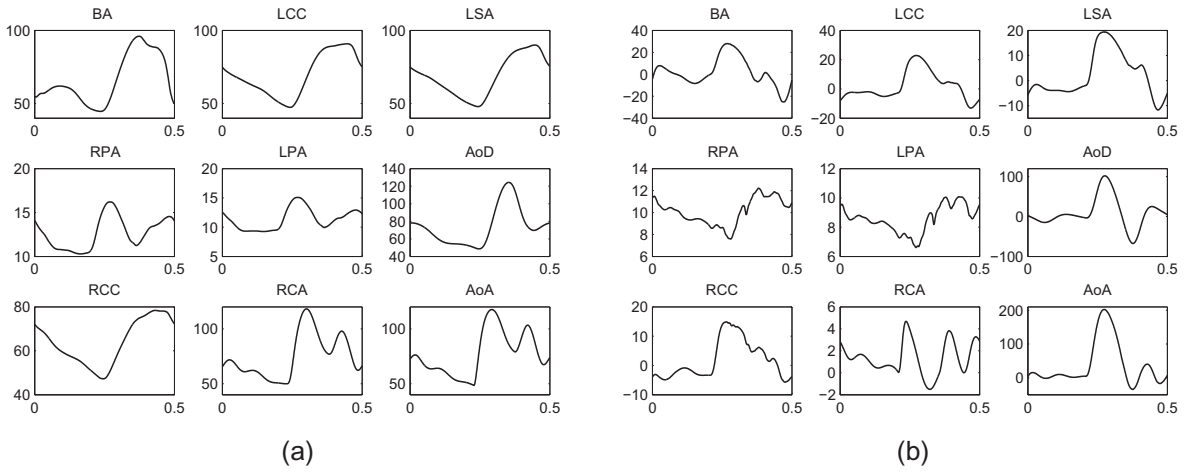

Fig. 11. Pressure (a) and flow rate (b) plots for the LPN shown in Fig. 10 for the coupled surfaces. Pressure plots are in mmHg versus time in seconds. Flow rate plots are in mL/s versus time in seconds.

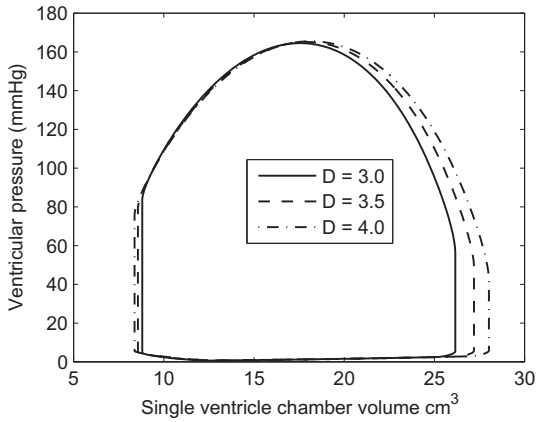

Fig. 12. Ventricular pressure-volume loop of the LPN shown in Fig. 10 with three different shunt sizes.

The resulting pressure and flow rate of the coupled surfaces are shown in Fig. 11. As expected, the results predict a lower pressure for the pulmonary branches compared to the systemic side. In contrast to the other branches, the coronary flow waveform has a second peak in diastole. There is significant backflow in the BA and RCC due to the shunt flow, which reduces the diastolic pressure in these branches.

To see the interaction of the two domains, the ventricular pressure-volume loop of three simulations with 3.0, 3.5, and 4.0 mm shunt (using the LPN and model shown in Fig. 10) is shown in Fig. 12. The 4.0 mm shunt diverts more blood to the pulmonary bed, which has a lower resistance compared to the systemic bed. Therefore, this geometry has lowest total resistance seen by the heart, which leads to the largest stroke volume, and hence the highest cardiac output. This example demonstrates the necessity of a coupled simulation for these types of case studies.

To compare the computational cost of the multi-domain method with monolithic boundary conditions, we also performed a simulation with the same geometry and resistance boundary conditions. The resistance values are tuned to obtain the same average pressure at the outlets as the multi-domain simulation. The LPN is replaced with resistance boundary conditions at the outlets and a prescribed uncoupled velocity, which is duplicated from the multi-domain simulation results, at the inlet of the ascending aorta. Comparing the computational costs of two methods for pure resistance boundary conditions, the partitioned approach cost 9% more. However, comparing to the simulation with Windkessel boundary conditions, the partitioned approach cost 9% less (44 min versus 48 min). These small differences indicate a negligible difference in cost between the proposed partitioned and monolithic approaches. The number of nonlinear iterations per cycle was almost the same (0.3% difference in number of iterations), which indicates insignificant differences between the two approaches.

For the original simulation with LPN shown in Fig. 10, five cardiac cycles were simulated with an average of 7.5 iterations per time step. This required 7,503 iterations per cycle in total, which took 38 min/cycle on a parallel 48 $\times$ 2.4 GHz processor cluster. Comparing these values to the case with pure resistance boundary conditions using a monolithic approach, the LPN

simulation required 22% more iterations per cycle, while each cycle cost 55% less overall. This is because the multi-domain problem has a tangent matrix with a lower condition number, which reduces the number of internal linear solver iterations, reducing its overall cost.

This example suggests the presented method can be used with multiple outlets and a complicated LPN with no significant additional computing cost. The semi-implicit implementation of the coupled Neumann boundaries formulation inside the iterative loop resulted in a stable solution with a time step size that is an order of magnitude higher than previous work, in which a similar problem was studied [34].

4. Discussion

The multi-domain approach presented in this work provides both detailed hemodynamic information in the 3D domain of interest, and global hemodynamic information in the circulatory system. We have presented a modular and flexible framework for coupling 3D finite element simulations to LPN models for cardiovascular simulation. In this framework, one can use either Dirichlet or Neumann coupled boundary conditions, depending on the type of LPN model employed. This method can be applied in a range of patient specific blood flow simulations, in which global information about circulatory dynamics is required. A separate numerical solver for the LPN, with a specific protocol for passing pressure and flow information at the boundaries, enables convenient implementation for legacy solvers in which the LPN can be changed or reconfigured without recompiling the 3D solver code.

Depending on the type of nonlinear elements in the 0D model, time step sizes, and other numerical parameters, either an implicit, semi-implicit, or explicit coupling approach can be used. Based on our results, the semi-implicit approach seems the most attractive choice, since it provides a more stable, yet cost-effective solution. In the explicit approach, a less costly scheme can be obtained that does not change the non-zero pattern of the sparse tangent matrix. However, this proves to be less stable with a lower convergence rate that increases the overall cost. By including only the diagonal part of $\boldsymbol{M}$ in the tangent matrix, which is generally a good approximation of the full matrix, we obtain a system of equations with good convergence. In doing so, off-diagonal elements of $\boldsymbol{M}$ that would decrease the sparsity of the tangent matrix and complicate parallelization of linear solver are neglected. Implementation of this approach requires only minor modifications to a Navier–Stokes solver in which simple boundary conditions such as resistance models are already implemented with a monolithic approach. Note that for these coupled Neumann boundaries, backflow stabilization allowed us to perform this coupling, where other methods may cause simulation divergence [19].

Conservation of mass can be directly satisfied through the external surfaces (via 0D domain), if the coupled Dirichlet boundary condition is imposed for all the external surfaces. Implementation of this method does not require any changes to the 3D solver, compared to a classic Dirichlet boundary condition other than passing the flow rate and pressure information. Comparing this approach with the Neumann approach we obtained improved convergence rates and stability, independent of the time-step size. On the other hand, the Dirichlet boundary condition approach requires knowledge of the velocity profile, which is not usually available. This requires an assumption that may change the local velocity solution and possibly the pressure field in the entire domain.

Use of a multi-domain method enables prediction of important hemodynamic parameters in the entire circulatory system that can be relevant to clinical decision making and surgical planning. One example is selecting between surgical options for single ventricle patients, in which prior explicitly coupled version of this method proved to be important for clinical applications [34–36]. In addition, the combination of this type of multi-domain simulation with formal design optimization methods provides a powerful tool that can assist in surgical planning, while accounting for the changing dynamic response of the heart and cardiovascular system [37].

Expanding this work to fluid structure interaction (FSI) simulation to model vessel wall deformation is an important topic for future investigation, although, beside Section 2.2.2, we expect the implementation to be essentially identical to what we have presented here [38,39,13]. Also, the dynamic response of an LPN can be modified to incorporate non periodic phenomena [9] and auto-regulatory mechanisms [40] to model exercise conditions. Due to the lack of available clinical data, specifying parameter values in an elaborate LPN is a challenging issue [41], and usually restricted to Windkessel type models [42–44].

Although, in comparison with 1D/3D coupling, the 0D/3D coupling cannot predict wave propagation, it is the only feasible option for modeling vessels outside of the 3D domain with no available geometrical information, as is often the case in image-based modeling. However we note that, the same implicit modular approach described in this work could be used for 1D/3D coupling.

5. Conclusion

We have presented a framework for coupling an arbitrary, user-defined lumped parameter network to a discretized 3D finite element domain, which exhibits the stability of monolithic approaches, while maintaining the flexibility and modularity of a partitioned approach. Two types of coupled boundaries, i.e. ‘Neumann’ and ‘Dirichlet’ boundary conditions, were discussed. The instability associated with backflow for the Neumann boundaries was addressed by adding an additional stabilization term to the formulation. In this formulation, at each nonlinear iteration of the Navier–Stokes solver, flow rates

of Neumann boundaries and pressures of Dirichlet boundaries are sent from the 3D to 0D domain, where ODE's are numerically integrated, and pressure or flow rate are passed back to the 3D domain. By using a finite difference technique to evaluate the 0D domain contribution to the tangent matrix of the 3D domain, a strongly coupled implicit formulation is proposed to improve the stability and convergence properties when using coupled Neumann boundaries. Good convergence properties were shown when accounting only for the effect of each Neumann surface on its own traction in the tangent matrix. Validating this framework against a Windkessel analytical solution demonstrated its accuracy; and strong stability properties were demonstrated through two case studies with closed-loop lumped parameter networks.

Acknowledgements

Funding for this work was provided by a Leducq Foundation Network of Excellent grant, an INRIA associated team grant, and a Burroughs Wellcome Fund Career Award at the Scientific Interface. The authors wish to thank Tain-Yen Hsia for providing the clinical impetus for the present work, Giancarlo Pennati, Francesco Migliavacca, and Sethuraman Sankaran for sharing their expertise in the LPN modeling.

Appendix A

Here, we provide a possible explanation for the numerically observed divergence of a simulation when a Neumann boundary is coupled to an inductor. In this case, the coupled surface pressure at each Newton iteration must be updated based on the flow rate,

$$\mathcal{P}_{(k)}^{n+1} = \mathcal{P}_d + L\frac{\Delta Q_{(k-1)}}{\Delta t}, \tag{43}$$

where $\mathcal{P}_{(k)}^{n+1}$ and $\mathcal{P}_d$ are the predicted pressure of the coupled surface for iteration k and distal point pressure (see Fig. 4). For infinitesimal changes, the following linear relationship is assumed between pressure and flow rate, which models the 3D domain behavior,

$$\Delta Q_{(k-1)} = -\lambda \Delta \mathcal{P}_{(k-1)}. \tag{44}$$

where, physically, λ is proportional to the reciprocal of vascular resistance. From Eqs. (43) and (44),

$$\mathcal{P}_{(k)}^{n+1} = \mathcal{P}_d - \frac{L\lambda}{\Delta t}\left(\mathcal{P}_{(k-1)}^{n+1} - \mathcal{P}^n\right). \tag{45}$$

This equation is unstable for $|L\lambda/\Delta t| > 1$. In practice, since $\lambda \neq 0$, the pressure of the coupled surface will oscillate and rapidly diverge for small time step sizes. Similarly for a Dirichlet boundary coupled to a capacitor, it can be shown that $Q_{(k)}^{n+1}$ will be an unstable function of $Q_{(k-1)}^{n+1}$.

References

[1] C. Taylor, C. Figueroa, Patient-specific modeling of cardiovascular mechanics, Annual Review of Biomedical Engineering 11 (2009) 109–134.
[2] C. Taylor, D. Steinman, Image-based modeling of blood flow and vessel wall dynamics: applications, methods and future directions, Annals of Biomedical Engineering 38 (2010) 1188–1203.
[3] G. Pennati, F. Migliavacca, G. Dubini, E. Bove, Modeling of systemic-to-pulmonary shunts in newborns with a univentricular circulation: state of the art and future directions, Progress in Pediatric Cardiology 30 (1–2) (2010) 23–29.
[4] I. Vignon-Clementel, A. Marsden, J. Feinstein, A primer on computational simulation in congenital heart disease for the clinician, Progress in Pediatric Cardiology 30 (2010) 3–13, http://dx.doi.org/10.1016/j.ppedcard.2010.09.002.
[5] N. Westerhof, F. Bosman, C.D. Vries, A. Noordergraaf, Analog studies of the human systemic arterial tree, Journal of Biomechanics 2 (2) (1969) 121–143.
[6] L. Formaggia, J. Gerbeau, F. Nobile, A. Quarteroni, Numerical treatment of defective boundary conditions for the Navier–Stokes equations, SIAM Journal on Numerical Analysis 40 (2002) 376–401.
[7] A. Quarteroni, A. Veneziani, Analysis of a geometrical multiscale model based on the coupling of ODEs and PDEs for blood flow simulations, Multiscale Model Simulations 1 (2) (2003) 173–195.
[8] I. Vignon-Clementel, C. Figueroa, K. Jansen, C. Taylor, Outflow boundary conditions for three-dimensional finite element modeling of blood flow and pressure in arteries, Computer Methods in Applied Mechanics and Engineering 195 (29–32) (2006) 3776–3796.
[9] I. Vignon-Clementel, C. Figueroa, K. Jansen, C. Taylor, Outflow boundary conditions for three-dimensional simulations of non-periodic blood flow and pressure fields in deformable arteries, Computer Methods in Biomechanics and Biomedical Engineering 13 (5) (2010) 625–640.
[10] H. Kim, I. Vignon-Clementel, C. Figueroa, J. Ladisa, K. Jansen, J. Feinstein, C. Taylor, On coupling a lumped parameter heart model and a three-dimensional finite element aorta model, Annual Review of Biomedical Engineering 37 (2009) 2153–2169.
[11] H. Kim, I. Vignon-Clementel, J. Coogan, C. Figueroa, K. Jansen, C. Taylor, Patient-specific modeling of blood flow and pressure in human coronary arteries, Annals of Biomedical Engineering 38 (2010) 3195–3209.
[12] C. Bertoglio, A. Caiazzo, M. Fenandez, Fractional-step schemes for the coupling of distributed and lumped models in hemodynamics, Research Report RR-7937, INRIA, Apr. 2012. <http://hal.inria.fr/hal-00690493>.
[13] S. Urquiza, P. Blanco, M. Venere, R. Feijoo, Multidimensional modelling for the carotid artery blood flow, Computer Methods in Applied Mechanics and Engineering 195 (33–36) (2006) 4002–4017.
[14] P. Blanco, R. Feijoo, S. Urquiza, A unified variational approach for coupling 3D–1D models and its blood flow applications, Computer Methods in Applied Mechanics and Engineering 196 (41–44) (2007) 4391–4410.
[15] A. Quarteroni, S. Ragni, A. Veneziani, Coupling between lumped and distributed models for blood flow problems, Computing and Visualization in Science 4 (2001) 111–124.
[16] J. Leiva, P. Blanco, G. Buscaglia, Iterative strong coupling of dimensionally-heterogeneous models, International Journal of Numerical Methods in Engineering 81 (12) (2010) 1558–1580.

[17] A. Malossi, P. Blanco, S. Deparis, A. Quarteroni, Algorithms for the partitioned solution of weakly coupled fluid models for cardiovascular flows, International Journal of Numerical Methods in Biomedical Engineering 27 (12) (2011) 2035–2057.
[18] D. Johnson, P. Naik, A. Beris, Efficient implementation of the proper outlet flow conditions in blood flow simulations through asymmetric arterial bifurcations, International Journal for Numerical Methods in Fluids 66 (11) (2011) 1383–1408.
[19] M.E. Moghadam, Y. Bazilevs, T. Hsia, I. Vignon-Clementel, A. Marsden, A comparison of outlet boundary treatments for prevention of backflow divergence with relevance to blood flow simulations, Computational Mechanics 48 (3) (2011) 277–291.
[20] C. Whiting, K. Jansen, A stabilized finite element method for the incompressible Navier–Stokes equations using a hierarchical basis, International Journal for Numerical Methods in Fluids 35 (1) (2001) 93–116.
[21] L. Franca, S. Frey, Stabilized finite element methods: II. The incompressible Navier–Stokes equations, Computer Methods in Applied Mechanics and Engineering 99 (2–3) (1992) 209–233.
[22] A. Brooks, T. Hughes, Streamline upwind/Petrov–Galerkin formulations for convection dominated flows with particular emphasis on the incompressible Navier–Stokes equations, Computer Methods in Applied Mechanics and Engineering 32 (1–3) (1982) 199–259.
[23] Y. Bazilevs, V. Calo, J. Cottrell, T. Hughes, A. Reali, G. Scovazzi, Variational multiscale residual-based turbulence modeling for large eddy simulation of incompressible flows, Computer Methods in Applied Mechanics and Engineering 197 (1–4) (2007) 173–201.
[24] K. Jansen, C. Whiting, G. Hulbert, A generalized-[alpha] method for integrating the filtered Navier–Stokes equations with a stabilized finite element method, Computer Methods in Applied Mechanics and Engineering 190 (3–4) (2000) 305–319.
[25] F. Shakib, T. Hughes, Z. Johan, A multi-element group preconditioned gmres algorithm for nonsymmetric systems arising in finite element analysis, Computer Methods in Applied Mechanics and Engineering 75 (1–3) (1989) 415–456.
[26] J. Schmidt, S. Delp, M. Sherman, C. Taylor, V. Pande, R. Altman, The simbios National center: systems biology in motion, in: Proceedings of the IEEE, Computational System Biology 96 (8) (2008) pp. 1266–1280 (special issue).
[27] E. Kung, A. Les, C. Figueroa, F. Medina, K. Arcaute, R. Wicker, M. McConnell, C. Taylor, In vitro validation of finite element analysis of blood flow in deformable models, Annals of Biomedical Engineering 39 (2011) 1947–1960.
[28] P. Kundu, I. Cohen, Fluid Mechanics, fourth ed., Academic press, 2008.
[29] H. Kim, C. Figueroa, T. Hughes, K. Jansen, C. Taylor, Augmented lagrangian method for constraining the shape of velocity profiles at outlet boundaries for three-dimensional finite element simulations of blood flow, Computer Methods in Applied Mechanics and Engineering 198 (45–46) (2009) 3551–3566.
[30] D. de Zelicourt, L. Ge, C. Wang, F. Sotiropoulos, A. Gilmanov, A. Yoganathan, Flow simulations in arbitrarily complex cardiovascular anatomies-an unstructured cartesian grid approach, Computers and Fluids 38 (9) (2009) 1749–1762.
[31] Y. Bazilevs, J. Gohean, T. Hughes, R. Moser, Y. Zhang, Patient-specific isogeometric fluid-structure interaction analysis of thoracic aortic blood flow due to implantation of the Jarvik 2000 left ventricular assist device, Computer Methods in Applied Mechanics and Engineering 198 (45–46) (2009) 3534–3550.
[32] F. Migliavacca, G. Pennati, G. Dubini, R. Fumero, R. Pietrabissa, G. Urcelay, E. Bove, T. Hsia, M. de Leval, Modeling of the Norwood circulation: effects of shunt size, vascular resistances, and heart rate, American Journal of Physiology-Heart and Circulatory Physiology 280 (2001) H2076–H2086.
[33] S. Sankaran, M.E. Moghadam, A. Kahn, E. Tseng, J. Guccione, A. Marsden, Patient-specific multiscale modeling of blood flow for coronary artery bypass graft surgery, Annals of Biomedical Engineering (2012).
[34] K. Lagana, R. Balossino, F. Migliavacca, G. Pennati, E. Bove, M. de Leval, G. Dubini, Multiscale modeling of the cardiovascular system: application to the study of pulmonary and coronary perfusions in the univentricular circulation, Journal of Biomechanics 38 (5) (2005) 1129–1141.
[35] F. Migliavacca, R. Balossino, G. Pennati, G. Dubini, T. Hsia, M. de Leval, E. Bove, Multiscale modelling in biofluiddynamics: application to reconstructive paediatric cardiac surgery, Journal of Biomechanics 39 (6) (2006) 1010–1020.
[36] A. Baretta, C. Corsini, W. Yang, I. Vignon-Clementel, A. Marsden, J. Feinstein, T. Hsia, G. Dubini, F. Migliavacca, Mocha, Virtual surgeries in patients with congenital heart disease: a multi-scale modelling test case, Philosophical Transactions. A. Mathematical, Physical, and Engineering Sciences 369 (1954) (2011) 4316–4330.
[37] M.E. Moghadam, F. Migliavacca, I. Vignon-Clementel, T. Hsia, A. Marsden, Optimization of shunt placement for the norwood surgery using multi-domain modeling, Journal of Biomechanical Engineering 134 (5) (2012) 051002.
[38] Y. Bazilevs, V. Calo, Y. Zhang, T. Hughes, Isogeometric fluid structure interaction analysis with applications to arterial blood flow, Computational Mechanics 38 (2006) 310–322.
[39] C. Figueroa, I. Vignon-Clementel, K. Jansen, T. Hughes, C. Taylor, A coupled momentum method for modeling blood flow in three-dimensional deformable arteries, Computer Methods in Applied Mechanics and Engineering 195 (41–43) (2006) 5685–5706.
[40] M. Olufsen, H. Tran, J. Ottesen, R. Program, L. Lipsitz, V. Novak, Modeling baroreflex regulation of heart rate during orthostatic stress, American Journal of Physiology-Regulatory, Integrative and Comparative Physiology 291 (5) (2006) R1355–R1368.
[41] S. Pope, L. Ellwein, C. Zapata, V. Novak, M. Kelley, M. Olufsen, Estimation and identification of parameters in a lumped cerebrovascular model, Mathematical Biosciences Engineering 6 (1) (2009) 93–115.
[42] G. Troianowski, C. Taylor, J. Feinstein, I. Vignon-Clementel, Three-dimensional simulations in glenn patients: clinically based boundary conditions, hemodynamic results and sensitivity to input data, Journal of Biomechanical Engineering 133 (11) (2011) 111006.
[43] G. Pennati, C. Corsini, D. Cosentino, T. Hsia, V. Luisi, G. Dubini, F. Migliavacca, Boundary conditions of patient-specific fluid dynamics modelling of cavopulmonary connections: possible adaptation of pulmonary resistances results in a critical issue for a virtual surgical planning, Interface Focus 1 (2011) 297–307, http://dx.doi.org/10.1098/rsfs.2010.0021.
[44] C. Bertoglio, P. Moireau, J. Gerbeau, Sequential parameter estimation for fluid structure problems: Application to hemodynamics, International Journal of Numerical Methods in Biomedical Engineering 28 (4) (2012) 434–455.